Title
Nonspecific labeling limits the utility of Cre-Lox bred CST-YFP mice for studies of corticospinal tract regeneration

Journal
The Journal of Comparative Neurology, 523(18)

ISSN
1550-7149

Authors
Willenberg, Rafer
Steward, Oswald

Publication Date
2015-12-15

DOI
10.1002/cne.23809

Peer reviewed

HHS Public Access

Author manuscript

J Comp Neurol. Author manuscript; available in PMC 2016 December 15.

Published in final edited form as:

J Comp Neurol. 2015 December 15; 523(18): 2665–2682. doi:10.1002/cne.23809.

Non-specific labeling limits the utility of Cre-Lox bred CST-YFP mice for studies of corticospinal tract regeneration

Rafer Willenberg[1,2] and **Oswald Steward**[1,2,3,4,*]

[1]Reeve-Irvine Research Center, University of California at Irvine, Irvine, California 92697

[2]Department of Anatomy & Neurobiology, University of California at Irvine, Irvine, California 92697

[3]Department of Neurobiology & Behavior, University of California at Irvine, Irvine, California 92697

[4]Department of Neurosurgery, University of California at Irvine, Irvine, California 92697

Abstract

Studies of axon regeneration in the spinal cord often assess regeneration of the corticospinal tract (CST). Emx1-Cre x Thy1-STOP-YFP mice have been reported to have yellow fluorescent protein (YFP) selectively expressed in forebrain neurons leading to genetic labeling of CST axons in the spinal cord, and it was suggested that these CST-YFP mice would be useful for studies of CST regeneration. Because regeneration past a lesion may involve only a few axons, the presence of labeled non-CST axons compromises interpretation. We show here that in CST-YFP mice, some YFP-labeled axons are not from the CST. Specifically, YFP-labeled axons are present in regions beyond those with anterogradely-labeled CST axons, most YFP-labeled axons beyond established CST locations do not undergo Wallerian degeneration following a large lesion of the sensorimotor cortex, some rubrospinal and reticulospinal neurons are labeled with YFP, and some YFP-labeled cells in the spinal grey matter have YFP-labeled projections into the spinal cord white matter. We further demonstrate that the density of YFP-labeled axon arbors hinders tracing of single axons to their point of origin in the main descending tracts. In light of recent advances in 3D imaging for visualizing axons in un-sectioned blocks of spinal cord, we also assessed CST-YFP mice for 3D imaging and found that YFP fluorescence in CST-YFP mice is faint for clearing-based 3D imaging in comparison to fluorescence in Thy1-YFP-H mice and fluorescence of mini-ruby BDA. Overall, the non-specific and faint YFP labeling in CST-YFP mice limit their utility for assessments of CST axon regeneration.

Graphical Abstract

*CORRESPONDENCE TO: Oswald Steward, Ph. D., 1105 GNRF, 837 Health Sciences Dr., University of California at Irvine, Irvine, CA 92697. osteward@uci.edu.

CONFLICT OF INTEREST

O. Steward is one of the co-founders of a company called “Axonis” which holds options on patents relating to PTEN deletion and axon regeneration. R. Willenberg declares no competing financial interests.

AUTHOR CONTRIBUTIONS

Author contributions: R.W and O.S. designed research, R.W. performed research; R.W. and O.S. analyzed data; R.W. and O.S. wrote the paper.

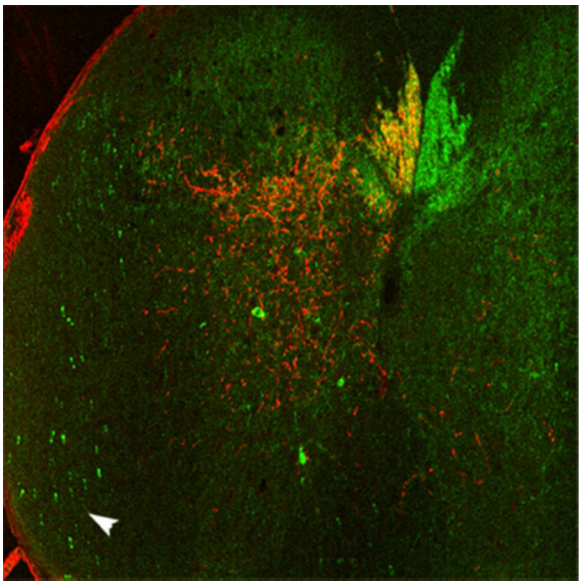

Keywords

CST; Cre; Emx1; spinal cord injury; transgenic

INTRODUCTION

Studies of axon regeneration following spinal cord injury often assess regeneration of the corticospinal tract (CST), which includes all axons that originate in the cerebral cortex and project into the spinal cord . Studies of the CST have commonly used anterograde tracers, which can specifically label CST axons but produce variable and incomplete labeling of the total complement of CST axons. Axonal labeling with tracer injections is transient, so the timing between tracer injection and euthanasia is critical, which complicates studies of axon regeneration after injury. As an alternative to anterograde tracing, Bareyre et al. (2005) used a Cre-Lox breeding system to create a mouse model in which cortical neurons express yellow fluorescent protein (YFP), leading to labeling of CST axons in the spinal cord—the CST-YFP mouse. In these mice, YFP labeling is conditional on expression of Cre driven by Emx1, which is selective for the embryonic forebrain (Simeone et al., 1992; Briata et al., 1996). Bareyre et al. proposed that these mice would be useful for studies of regeneration of CST axons because the permanent genetic labeling is independent of tracer injections and all CST axons in these mice are labeled with YFP.

For unambiguous interpretation of CST regeneration, it is important that genetic labeling be specific to the CST. Regeneration may involve only a few axons, and these may extend into locations outside the territory of normal CST axons (Steward et al., 2003). For this reason, the presence of even a few YFP-labeled non-CST axons can compromise interpretation. In CST-YFP mice, Bareyre et al. report YFP-labeling of axons in the spinal cord in locations where the mouse CST had not been previously described (2005). Though these axons might be CST axons outside of the main tracts (ectopic axons), another possibility is YFP labeling

of non-CST axons. A previous study also proposed the possibility of YFP-labeling of non-CST axons (Galley and Clowry, 2010), but YFP-labeled neurons outside of the cortex were not confirmed to project axons into the spinal cord. Labeling of non-CST axons with YFP would limit the utility of CST-YFP mice for studying CST regeneration.

Here, we provide a critical evaluation and characterization of CST-YFP mice for studying CST regeneration. First, we show that in adult CST-YFP mice, YFP is not specific to the CST. We show that some YFP-labeled axons in the spinal cord do not degenerate following cortical lesions, some neurons in the spinal cord gray matter have YFP-labeled projections into the white matter, and some rubrospinal and reticulospinal neurons are labeled with YFP.

In addition, although it is advantageous that most or all CST axons express YFP for assessing the entire population of CST axons, we show that the density of labeled axon arbors in the spinal cord makes it difficult to trace individual axons. This hinders tracing axons back to the main CST bundle to determine their point of origin, an important approach for concluding that the axons actually branch from injured axons [see (Tuszynski and Steward, 2012)].

Finally, in light of recent advances in 3D imaging of fluorescently-labeled axons in unsectioned spinal cords (Ertürk et al., 2012b), we assessed CST-YFP mice using clearing-based 3D imaging and found that nascent YFP fluorescence in CST-YFP mice is faint for 3D imaging in comparison to fluorescence in Thy1-YFP-H mice and fluorescence of mini-ruby BDA-labeled axons. Overall, our results reveal limitations of CST-YFP mice for studying CST regeneration, and highlight issues that may limit the general usefulness of genetic labeling for assessing tract-specific axons.

MATERIALS AND METHODS

All animal procedures were approved by the Institutional Animal Care and Use Committee (IACUC) at the University of California, Irvine.

Mice

CST-YFP mice were created by crossing Emx1-Cre mice [B6.129S2-*Emx1*$^{tm1(cre)Krj}$/J, Jackson Labs, RRID: MGI_2684610] to Thy1-STOP-YFP mice [B6.Cg-Tg(Thy1-EYFP)15Jrs/J, Jackson Labs, RRID: MGI_3707420] as described by Bareyre et al. (2005). Emx1-Cre mice have Cre expression driven by endogenous *Emx1* and facilitated by an internal ribosome entry site (IRES) sequence (Gorski et al., 2002). Thy1-STOP-YFP mice have YFP expression driven by neuronal *Thy1* following excision of the floxed STOP cassette (Buffelli et al., 2003). Both parent lines had been backcrossed to C57BL/6 mice. Progeny of the parental cross were thus hemizygous for both *Emx1-Cre* and *Thy1-STOP-YFP*, with the transgenic design to yield YFP expression in all cells expressing both Emx1 and neuronal Thy1.

A total of 25 adult CST-YFP mice of both sexes were analyzed for this study including 4 naive mice that had no injury or tracer injection, 4 that had cortical lesions, 3 that had received Fluoro-Gold (FG) injections into the spinal cord to identify cells of origin of

descending spinal pathways, and 14 that received intra-cortical injections of BDA to trace the CST. Two Thy1-YFP-H mice (one homozygous and one hemizygous) [B6.Cg-Tg(Thy1-YFP)HJrs/J, Jackson Labs, RRID: MGI_3497947] and one PTEN-floxed (*Pten*$^{f/f}$) mouse [C; 129S4-*Pten*^{tm1Hwu}/J, Jackson Labs, RRID: MGI_2156086] with BDA labeling of CST axons were also used for 3D imaging analysis.

Motor cortex lesions

CST-YFP mice (n=4) received unilateral cortical lesions to assess anterograde degeneration of CST axons in the spinal cord. Lesions were unilateral in order to detect the laterality of degenerating axons from one cortex. Cortical lesions were guided by mapping CST origins based on retrograde labeling with Fluoro-Gold (Steward and Willenberg, unpublished observations) and performing the lesions with the aim to include all cortical areas containing neurons that give rise to the CST. Mice were anesthetized with an intraperitoneal injection of mixed ketamine (100 mg/kg) and xylazine (10 mg/kg). The scalp was incised and the skull overlying the dorsal right cortex was removed from near midline to the temporalis muscle. Care was taken to avoid damaging the sagittal and transverse sutures and underlying venous sinuses. The cortex was gently aspirated using a pulled Pasteur pipette with a tip diameter of approximately 300 μm, down to the level of sub-cortical white matter. The ablated area extended approximately 4 mm medio-laterally and 5–6 mm rostro-caudally. The scalp was sutured with 5-0 silk, and mice survived for 1 week before being humanely killed by an overdose of Euthasol®. Mice were transcardially perfused with 4% paraformaldehyde in phosphate buffer (PFA), and brains and spinal cords were post-fixed overnight and stored in 27% sucrose.

Tract tracing

Biotinylated dextran amine (BDA) was injected to anterogradely label axons of the CST. Unilateral intracortical injections of mini-ruby BDA (10,000 MW, 10% in dH_20, Invitrogen) were made in stereotaxic coordinates into the left or right sensorimotor cortex. Injections were targeted to forelimb and hindlimb regions with coordinates overlying primary motor cortex, as presented by Paxinos (2004). Coordinates were 0.5 mm deep, 1.0 mm lateral, and 0.5 mm rostral, 0.2, 0.5, and 1.0 mm caudal to bregma (0.4 μl per site). Mice were humanely killed and transcardially perfused as above, 2–3 weeks post-injection.

Retrograde labeling

To identify non-CST neurons that project to the spinal cord, Fluoro-Gold (Fluorochrome, LLC) was injected into the spinal cord of CST-YFP mice (n=8). Briefly, mice were anesthetized with isofluorane, and a laminectomy was performed at cervical level 5 (C5) to expose the underlying spinal cord. Injections of 4% Fluoro-Gold (FG) were made bilaterally 0.5 mm lateral to midline and 0.6 mm deep using an electronically-controlled injection system (Nanoliter 2000 injector and Micro4 pump controller, World Precision Instruments) with pulled glass micropipettes. Initially mice received injections of 0.4 μl per site. During recovery from anesthesia, mice exhibited unusual symptoms involving tonic limb extension with trembling, fixed postures and dorsiflexion of the tail, and one of the first 2 mice with 0.4 μl injections died the same afternoon. The spasms and death following injections of FG

into the cervical spinal cord are an animal welfare issue. In this regard, it is noteworthy that there have been previous reports of neurotoxicity from FG (Schmued et al., 1993; Naumann et al., 2000). To address this, 5 mice were injected with smaller volumes of FG (0.2 µl per site). Four of the 5 mice exhibited spasms though they were less pronounced, and one died later the same day. To test whether the spasms were due to the method of using the electronically-controlled injection system, an additional mouse was injected with 0.4ul FG by Hamilton syringe tipped with a pulled glass micropipette, and this mouse also had subsequent spasms. Mice that recovered did not exhibit obvious behavioral abnormalities. One week following injections, mice were transcardially perfused with 4% PFA, and brains and spinal cords were dissected and post-fixed in 4% PFA overnight before being equilibrated and stored in 27% sucrose. Two mice with 0.4 µl injections and 3 mice with 0.2 µl injections had robust labeling, and the larger cohort (with 0.2 µl injections) was used for analysis.

As a technical aside, we have carried out follow-up studies testing lower concentrations of FG, which demonstrated that 6 out of 6 mice injected with lower concentrations of FG (1%) exhibited less intense and shorter spasms during recovery from anesthetic, and there were no deaths.

Histology

Sectioning—Tissue was cryoprotected via equilibration in 27% sucrose, frozen in TissueTek O.C.T. (Sakura Finetek), and sectioned on a cryostat at 30 µm for the retrograde tracing and degeneration studies and at 20 µm for all other studies. Spinal cord cross sections were collected from all intact specimens and those injected with BDA. Sagittal sections were also collected from 6 mouse spinal cords with BDA tracing. Horizontal sections were collected from all of the spinal cords of mice with cortical lesions and 2 spinal cords with BDA tracing. Coronal brainstem sections were collected from mice with retrograde FG labeling.

Signal amplification—Native YFP fluorescence in CST-YFP mice appears weak for individual axons, so sections were immunostained using antibodies raised in rabbit against green fluorescent protein (GFP) and secondary antibodies conjugated to Alexa-488, as described (Bareyre et al., 2005). Sections were washed three times in phosphate-buffered saline (PBS), blocked in 5% normal goat serum (Vector Biolabs, Philadelphia, PA) in PBS, and then incubated overnight in a 1:250 dilution of rabbit anti-GFP (Millipore, Cat# AB3080, RRID: AB_91337) in 5% normal goat serum and PBS. Sections were washed 3 times in PBS, incubated in a 1:250 dilution of Alexa Fluor® 488 (Life Technologies) in PBS for 2 hours, then washed a final 3 times before slide mounting and cover slipping with VectaShield® (Vector Biolabs) or Kaiser's glycerol jelly mounting medium.

In select slides of specimens with mini-ruby BDA injections, BDA was amplified by staining with a tyramide signal amplification (TSA) kit with Cy3 conjugation (PerkinElmer, Waltham, MA). Endogenous peroxidases were quenched with 3% peroxide in tris-buffered saline (TBS; 100mM Tris, 150mM NaCl, pH 7.4) for 15 minutes and then washed twice in TBS before blocking in TSA-kit blocking buffer for 30 minutes. Slides were then incubated

with a 1:100 dilution of streptavidin-horseradish-peroxidase (SA-HRP) for 2 hours, then washed 3 times in TBS with 0.05% Tween® 20 (Sigma Aldrich, St. Louis, MO). TSA detection was performed by adding a 1:50 dilution of Cy3-tyramide in substrate amplification diluent for 30 minutes in humid incubation, followed by washing TBS with 0.05% Tween® and cover-slipping using Kaiser's mounting medium.

Antibody characterization—Specificity of the anti-GFP antibody is demonstrated by the fact that immunostaining of sections from mice that do not express fluorescent protein reveals no staining (Schaefer et al., 2005).

Fluorescent Nissl-like staining—To identify cytoarchitectural borders in midbrain sections of specimens with FG labeling, selected brain sections were stained with NeuroTrace® (Life Technologies). Sections were washed in PBS with 0.1% Triton X-100 (Sigma Aldrich), 2x in PBS, then incubated in 1:50 dilution of blue NeuroTrace® for 20 minutes with agitation. Sections were again washed in PBS with Triton and then 2x in PBS before being mounted and coverslipped with VectaShield® (Vector Biolabs).

Epifluorescent and confocal imaging

Epifluorescent imaging was performed on an Olympus AX-80 microscope, and confocal imaging was performed on an Olympus Fluoview FV1000. For hi-resolution images wider than the viewfield, overlapping images were collected and stitched together in ImageJ (RRID: nif-0000–30467; Rasband, 1997) using the linear blending fusion method of the Preibisch stitching plugin (Preibisch et al., 2009). In confocal images of longitudinal spinal cord sections from mice with cortical lesions, background speckling noise was reduced to enhance the distinction of degenerated axon fragments by using ImageJ's remove outliers function (radius 0.5 px, threshold 50).

Clearing and 3D imaging

3D imaging was performed on blocks of spinal cord from CST-YFP mice, Thy1-YFP-H mice, and a PTEN-floxed (*Pten*$^{fl/fl}$) mouse with CST axons labeled with mini-ruby BDA. The block of spinal cord from the *Pten*$^{fl/fl}$ mouse was taken rostral to a dorsal hemisection spinal cord injury at T12 and had received cortical injections of AAV-Cre (as described in Liu et al. (2010)), as part of a prior CST regeneration experiment. The area analyzed was far rostral to the injury and presumably reflects normal CST axon distribution. Blocks of spinal cord were progressively dehydrated and defatted in tetrahydrofuran (50%, 80%, and 3× 100%, Sigma Aldrich) and dichloromethane (Sigma Aldrich) before clearing in a mixture of benzyl alcohol (Sigma Aldrich) and benzyl benzoate (Sigma Aldrich) in a 1:2 ratio (BABB), as described (Ertürk et al., 2012b). Specimens were placed in the BABB clearing solution in a chamber made by silicone isolators (Grace Bio-Labs, #664207) sandwiched by a glass microscope slide and coverslip. Specimens were then imaged in transverse and horizontal orientations on a 3i Vivo 2-photon microscope equipped with a Zeiss 20x objective with 1.0 numerical aperture. Imaging was of nascent fluorescence, without antibody enhancement or any signal amplification.

Quantification of YFP-labeled axons after unilateral cortical ablation

In specimens with cortical ablations (n=4), we characterized and quantified YFP-labeled axons in the dorsolateral white matter (DL) based on morphology. Axons in the DL that were visibly continuous and lacked distributed swellings were categorized as intact. Discontinuous axons appearing as ovoids (Lubińska, 1977; Griffin et al., 1992), or with breaks and swellings were categorized as fragmented. As axonal beading has been documented in the progression of Wallerian degeneration in the central nervous system (Kerschensteiner et al., 2005; Beirowski et al., 2010) including of the CST (Kalil and Schneider, 1975), continuous axons with distributed swellings were categorized separate from intact axons, as being beaded.

In horizontal sections, confocal image stacks at 40X magnification of dorsolateral white matter extending from a cut edge of the mid-cervical horizontal sections were analyzed from every 3rd section from the dorsal extent of the lateral column down to the level of the central canal. One specimen was cut off-axis, and was excluded from this quantification. In ImageJ, axons crossing a line drawn at 200 μm from the cut edge were categorized and quantified through the stack. Only axons distinctly in the white matter were quantified, consequentially omitting any dlCST axons that remained in fascicles in the adjacent grey matter in the mid-cervical sections (Steward et al., 2004). An optical dissector method (Guillery, 2002) was employed by excluding axons present in a lookup section within each stack. The number of dorsolateral axons was then extrapolated by multiplying the raw counts by 3. The mean number of dorsolateral axons ipsilateral vs. contralateral to the lesion for each categorized type were assessed by Bonferroni post-hoc tests following a 2-way mixed-model ANOVA using GraphPad Prism® (GraphPad Software, RRID: rid_000081).

In the ventral spinal cord, quantification of axons was performed in cross sections to maintain regularity in quantification throughout the spinal cord's ventral and lateral extremes. This avoided adjusting parameters of quantification in oval or irregularly shaped sections that are commonly produced through longitudinal sectioning at or near the circumferential edges of the spinal cord (an imperfect cylinder). Cross sections of mid-cervical spinal cords from specimens with cortical ablations (n=4) and uninjured controls (n=3) were analyzed at 20X magnification in stitched image stacks in ImageJ. Stitched images were rotated to align midline to the vertical axis, and a horizontal line was overlaid through the central canal to define the dorsal vs. ventral spinal cord. A perpendicular line was overlaid ventrally from the central canal to laterally divide the ventral column (VC), and 2 additional lines were overlaid extending from the central canal 30° bilaterally from midline approximately along the medial border of each ventral horn to delineate the ventral lateral white matter (VL) from the ventral column on either side (Fig. 2*B*). Analysis in confocal image stacks permitted virtual focusing along the z-axis and quantification of axons appearing to be continuous within each section. Ipsilateral and contralateral axons and axons from one side of controls in each respective ventral region were averaged from 3 sections per animal. Quantified axons from the VL and VC regions were each analyzed by ANOVA using GraphPad Prism®.

Quantification of identified rubrospinal and reticulospinal YFP-labeled neurons—Coronal midbrain sections of CST-YFP mice injected with FG were examined for cells labeled with FG in the red nucleus and other brain regions, and FG-labeled cells in these sections were analyzed for co-labeling with YFP. Co-labeled cells in the red nucleus and reticular formation were quantified in every 7th section through a standardized volume of midbrain encompassing the red nucleus, beginning at the supramamillary decussation and extending 1.5 mm caudally. The red nucleus and other midbrain regions were identified by cytoarchitectural borders from blue fluorescent Nissl-like staining (NeuroTrace®), neuroanatomical landmarks, and reference to the Allen Mouse Brain Atlas, ©2012 Allen Institute for Brain Science, RRID: nif-0000–00508 [Internet, available from: http://mouse.brain-map.org/]. Estimates of the total number of co-labeled cells were made by multiplying raw counts by the inverse of the fraction of sections quantified and the Abercrombie correction factor (Abercrombie, 1946; Guillery, 2002).

Axon tracing assessment

YFP-labeled axons were assessed for traceability in grey matter by using an axon tracing task performed by 4 individuals. Stacks of confocal images from horizontal sections of spinal cord imaged at 40X and with 0.5 μm spacing were analyzed in ImageJ. Three BDA-labeled axons with long discontinuous segments and YFP co-labeling were selected for tracing in the densely YFP-labeled grey matter, and an additional axon was selected to familiarize individuals with the task. Following the familiarization with the task, 4 individuals were instructed to trace each axon within a stack of images from a designated starting point. Two individuals had experience studying labeled axons in the spinal cord and two did not (novice). None of the individuals had seen the selected images before, and each were presented with each image stack to trace each axon based on only YFP-labeling first, and BDA-labeling second. A tracing's extent was marked with the cursor point tool in ImageJ. A line was drawn from the cursor point to the starting point, and the length of this line was measured in ImageJ and recorded as the distance that the axon was traced. The BDA vs. YFP tracing lengths were analyzed by paired t-test using GraphPad Prism®.

RESULTS

In their original publication, Bareyre et al. report complete and specific YFP-labeling of CST axons in the spinal cord, but also document YFP-labeled axons in locations previously not established for the mouse CST (2005). These locations include the ventral column, where the CST is established in rats but not in mice, and the ventral lateral white matter. We define mouse non-CST locations to be the ventral column and ventral part of the lateral white matter.

All of the CST-YFP mice that were examined in the present study had YFP-labeled axons with a similar distribution. Labeled axons were present in the expected locations of the CST in the dorsal column and dorsolateral column as well as the non-CST locations of the ventral part of the lateral white matter and the ventral column. To estimate the number of YFP-labeled axons in these non-CST locations, we counted the number of YFP-labeled axons that were ventral to the central canal in mid-cervical sections on one side, and multiplied by 2 to

account for both sides. This yielded an estimate of 128 ± 22 (mean ± SEM, n=3) YFP-labeled axons in non-CST locations.

YFP labeling vs. anterograde CST tracing

YFP-labeled axons in unexpected locations might be ectopic CST axons, or non-CST axons from other neurons that express YFP. To begin to test these possibilities, we injected mini-ruby biotinylated dextran amine (BDA) into the right sensorimotor cortex to anterogradely label CST axons.

Intra-cortical BDA injections in CST-YFP mice, which have a mixed C57Bl/6 background, produced a pattern of CST labeling in the spinal cord comparable with what has been previously reported in C57Bl/6 mice (Inman and Steward, 2003; Steward et al., 2004, 2008) and mice on a C57Bl/6 background (Coonan et al., 2001). Figure 1 illustrates the pattern of BDA and YFP labeling in the low cervical and upper thoracic spinal cord. In panels A-F, BDA signal was amplified with tyramide signal amplification (TSA) and imaged with confocal microscopy. (For magenta-green confocal panels, see Suppl. Fig. S1) Large numbers of BDA-labeled axons (red) are present in the dorsal column on the left and a smaller number of BDA-labeled axons are present in the dorsal part of the lateral column on the same side (Fig. 1*A*,*E*), corresponding to the dorsal CST (dCST) and dorsolateral CST (dlCST), respectively (Steward et al., 2004, 2008). In one of 14 mice, a few BDA-labeled axons coursed longitudinally in the ventral column contralateral to the labeled dCST (ipsilateral to the injected cortex), in the location of the ventral CST seen in rats (Fig. 1*G*,*N*, without BDA amplification) (Brösamle and Schwab, 1997; Steward et al., 2008; Lang et al., 2012).

YFP-labeled axons were also present in the dorsal, lateral, and ventral columns, (Fig. 1*B*,*M*). In the dorsal lateral column, however, YFP-labeled axons were present farther lateral and ventral than the BDA-labeled dlCST axons (Fig. 1*E*,*F*). Some of these YFP-labeled axons appeared distinctly thicker than those in the region of dlCST axons labeled with BDA. YFP-labeled axons were also present in the ventral lateral columns (Fig. 1*B*,*C*,*H*,*J*) and sparsely distributed in the ventral column. BDA-labeled axons were not observed coursing in these non-CST locations (Fig. 1*A*,*D*,*I*,*K*). Thus, BDA labeling of CST axons in CST-YFP mice is comparable to patterns previously reported for the mouse CST, whereas YFP-labeled axons were present beyond the regions of BDA-labeled axons in locations where CST axons have not been reported.

Ablation of the sensorimotor cortex does not lead to Wallerian degeneration of YFP-labeled axons outside the expected distribution of the CST

Conceivably, our BDA injections may have missed some part of the sensorimotor cortex that gives rise to the YFP-labeled axons in atypical locations. To provide a complementary approach to testing whether all YFP-labeled axons are of the CST, we assessed whether large cortical lesions led to Wallerian degeneration of YFP-labeled axons in non-CST locations.

Locations of CST origins were confirmed by retrograde labeling of cortical neurons following injections of Fluoro-Gold (FG) into the cervical spinal cord (not shown). Previous studies have shown that cervical injections of FG in rats labeled both forelimb and hindlimb regions of sensorimotor cortex (Nielson et al., 2011), presumably reflecting uptake by axons of passage as well as axon terminals (Schmued and Fallon, 1986; Ambalavanar and Morris, 1989; Dado et al., 1990; Qu et al., 2006). The distribution of FG-labeled cortical neurons was comparable to that previously reported in mice (Liang et al., 2011). A cortical map made from the spans of regions of labeled cells (Willenberg and Steward, unpublished observations) was used to guide our unilateral cortical lesions to include all cortical regions with neurons that give rise to the CST, although we cannot exclude that some CST neurons may have remained.

Figure 2*A* illustrates the extent of the lesion in one mouse. Wallerian degeneration of YFP-labeled axons was assessed in the mid-cervical spinal cord (approx. C3-C4) in the areas indicated in Fig. 2*B*. The dorsal column (DC), dorsal part of the lateral column (DL) and ventral column (VC) contain the dCST, dlCST, and vCST respectively. The part of the lateral column ventral to the central canal (VL in Figure 2) contains YFP-labeled axons, but is not known to contain CST axons. Panels C-H illustrate confocal images of horizontal sections through the respective areas. One week after lesions of the right sensorimotor cortex, YFP-labeled axons exhibiting signs of Wallerian degeneration were present in the expected locations of CST axons including the left DC and DL (Fig. 2*C*&*D*). Wallerian degeneration was evidenced by axonal fragmentation and beading which are characteristic of degenerating CNS axons (Waller, 1850; Lubińska, 1977; Kerschensteiner et al., 2005; Beirowski et al., 2010) including of the CST (Kalil and Schneider, 1975). YFP-labeled axons appeared intact in the right dorsal column (Fig. 2*C*), and no intact YFP-labeled axons were seen in the left dorsal column.

Although fragmented axons were evident in the dorsal part of the lateral column on the left, there were also intact YFP-labeled axons in the same region, especially just lateral to the ones that were fragmented (Fig. 2*D*, arrow). Most YFP-labeled axons in the dorsolateral column on the right appeared intact (Fig. 2*E*), although a few fragmented axons were seen, consistent with degeneration of the small number of uncrossed dCST and dlCST axons (Brösamle and Schwab, 1997; Steward et al., 2004, 2008; Zheng et al., 2006). Occasional YFP-labeled axons also appeared as beaded in non-injured control mice (not shown). The number of intact, beaded, and degenerated axons were not significantly different between the left and right sides (all $p > 0.05$, Bonferroni post-hoc tests following 2-way mixed-model ANOVA, n=3; Fig. 2*I*).

There were a few beaded and fragmented YFP-positive axons in the right ventral column in the position of the vCST, but most YFP-positive axons in the ventral column and the ventral lateral columns appeared intact (Fig. 2*F*-*H*). There were no significant differences between sides in the number of intact YFP-labeled axons in the lateral column ventral to the central canal ($p=0.671$, ANOVA, n=4; Fig. 2*J*) or ventral column ($p=0.627$, ANOVA, n=4; Fig. 2*K*) or relative to one side of non-injured control mice (n=3).

Because unilateral cortical lesions deplete CST axons on one side, the remaining YFP axons on the side contralateral to the lesion provide an estimate of non-CST axons on one side. Adding the intact axons on the left from the DL in Fig. 2*I* to those in the left VL and VC from the same 3 of the 4 animals assessed in Fig. 2*J* & 2*K* yields 136 ± 16 (mean ± SEM) intact YFP-labeled axons on the left side. Based on this, the total on both sides is estimated to be 272 ± 32 (mean ± SEM) YFP-labeled non-CST axons.

Some non-CST cells that project to the spinal cord express YFP

If non-CST axons are labeled with YFP in the spinal cord, then these axons must arise from neurons outside of the cortex. As reported by Bareyre et al. (2005), a few YFP-positive neurons were present in the spinal gray matter in our tissue (Figure 1*G*, arrowhead). Other examples are shown in Figure 3 both in cross section (Fig. 3*A*) and horizontal sections (Fig. 3*B–K*), with some imaged by confocal microscopy (Fig. 3*I–K*). YFP-labeled axons could be followed from some of these neurons into the white matter in both uninjured mice (Fig. 3*A–H*) and mice with cortical lesions (Fig. 3*I–K*), and some projections extended both rostrally (Fig. 3*B,K*), and caudally (Fig. 3*G,I,J*). Projections of YFP-labeled neurons were observed in the ventral medial and lateral white matter. Additionally, one axon extending from the lateral white matter was identified coursing in a ventral root and exiting the spinal cord (Fig. 3*D*), suggesting YFP-labeling of a motoneuron axon. Hence, some neurons in the spinal grey matter contribute YFP-labeled projections into the white matter of the CST-YFP spinal cord.

To identify other possible sources of YFP-labeled non-CST axons in the spinal cord, we first examined brain sections for YFP-labeled neurons outside of the cortex. Scattered YFP-labeled cells were present in most brain regions examined, including the red nuclei, superior colliculi, reticular formation, and vestibular nuclei, which are brain nuclei with major descending projections to the spinal cord.

To test the hypothesis that descending non-CST axons express YFP, we injected the retrograde tracer Fluoro-Gold (FG) into the cervical spinal cord of CST-YFP mice, and examined FG-labeled brain cells outside of the cortex for co-labeling with YFP. In midbrain sections of each of the 3 mice examined, YFP-labeled cells co-labeled with Fluoro-Gold were identified by confocal microscopy in the red nucleus and the reticular formation (Fig. 4, magenta-green version in Suppl. Fig. S2). A very small number of co-labeled cells were also present in the periaqueductal grey (not shown), consistent with previous studies (Mantyh and Peschanski, 1982; Liang et al., 2011). A raw average of 22.7 co-labeled rubrospinal and 17.0 co-labeled reticulospinal neurons (StdDev 11.6 and 14.4, respectively) were identified per mouse, with an estimated total average of 89 rubrospinal and 66 reticulospinal co-labeled neurons in 1.5 mm of midbrain for the 3 animals (Fig. 4*G*). This quantification does not present an absolute number of YFP-labeled rubrospinal and reticulospinal neurons, but rather confirms that some rubrospinal and reticulospinal neurons are labeled with YFP. These results confirm YFP-labeling of some non-CST neurons that project to the spinal cord in CST-YFP mice.

Dense and faint YFP labeling impedes individual axon visualization and tracing

With some YFP-labeled non-CST axons, one way to confirm CST origins is by tracing axons back to the main tract. Tracing axons back to a cut parent tract can also support that the axons had regenerated (Tuszynski and Steward, 2012). In CST-YFP mice, however, the density of YFP-labeled axons is high especially adjacent to the dorsal column, which is the location through which axons would need to be traced to confirm origins from CST axons in the dorsal column. Figure 5 illustrates the grey matter adjacent to the dorsal column. (Suppl. Fig. S3 shows the figure with magenta-green confocal panels.) YFP-labeling of many axons is also faint, such that under epifluorescence microscopy at 20X magnification, YFP-labeling was not evident in some CST axons labeled with BDA (Fig. 5*A–B*), though the same CST axons were confirmed to have YFP co-labeling under confocal microscopy at 40X magnification (Fig. 5*C–E*).

To compare the ability to trace YFP vs. BDA-labeled axons, 4 individuals were asked to trace selected co-labeled axons in a stack of confocal images from uninjured mice, first using YFP and then BDA imaging. One of these axons extending from the dCST into the grey matter was traced by all 4 individuals into the grey matter based on BDA labeling, but none of the individuals traced the axon beyond the grey matter interface based on labeling with YFP (Fig. 5*F–H*). Other axons were also traced incompletely under visualization by YFP as compared to BDA (Table 1). In three instances, individuals' tracing ended on incorrect YFP-labeled axons, whereas this only occurred in one case based on BDA-labeling (Table 1). Individuals with experience in tracing axons were generally able to trace YFP-labeled axons farther than the novices. Overall tracings based on visualization by YFP were significantly shorter than tracings by visualization by BDA ($p = 0.0402$, two-tailed paired t-test), as were tracings in which incorrectly traced axons were excluded ($p = 0.0491$, two-tailed paired t-test). These results indicate that visual tracing of YFP-labeled CST axons is impeded in the densely YFP-labeled grey matter adjacent to the main CST.

Nascent YFP fluorescence in CST-YFP mice is faint for 3D imaging relative to fluorescence in Thy1-YFP-H mice and mice with mini-ruby BDA labeling

Recent advances in tissue clearing have allowed imaging and 3D reconstructions of fluorescent axons deep in un-sectioned tissue (Hama et al., 2011; Ertürk et al., 2012a; b; Chung et al., 2013; Ke et al., 2013; Kuwajima et al., 2013; Tomer et al., 2014; Yang et al., 2014). 3D imaging is especially promising for regeneration studies as it enables evaluation of candidate regenerated axons along their continuous course, rather than relying on reconstructions from axon segments. With the extensive genetic labeling in CST-YFP mice, this approach could be useful for initial screening of axon growth following injury. To evaluate the utility of CST-YFP mice for 3D imaging, we used the protocol of Ertürk et al. (2012b), which can rapidly render spinal cords clear (in a few hours) and has been used for imaging axons in the spinal cord following injury. Blocks of spinal cord from CST-YFP mice, Thy1-YFP-H mice, and a mouse with mini-ruby BDA-labeling of CST axons were cleared and imaged as in Ertürk et al. (2012b), using 2-photon microscopy. To maintain consistency in comparison, a hemizygous Thy1- YFP-H mouse was also assessed as CST-YFP mice are hemizygous for Thy1-driven YFP expression.

As demonstrated previously in rat (Ertürk et al., 2012b), mini-ruby BDA-labeled CST axons are evident in 3D reconstructions (Fig. 6*A*, arrow); individual BDA-labeled axons are evident in the dorsal column in a thin projection (Fig. 6*B*), and one labeled axon can be seen in the gray matter (arrow). This is from a block of cervical spinal cord rostral to a low-thoracic lesion in a PTEN-floxed mouse that was injected with AAV-Cre as in Liu et al. (2010). PTEN deletion leads to sprouting of CST axons just rostral to the lesion and regeneration of axons past a lesion, but there are no obvious differences in the extent of BDA labeling far rostral to the injury relative to that in control mice. The question of whether PTEN deletion leads to better BDA labeling has not been tested directly, however.

After empirically determining 2-photon laser excitation wavelength to be optimal at ~950 nm for our YFP-labeled specimens, cleared blocks of spinal cord from CST-YFP and Thy1-YFP-H mice were imaged using this laser wavelength and the same scan settings. In a hemizygous Thy1-YFP-H mouse, labeled axons were evident in the dorsal column and distributed through the white matter (Fig. 6*C–D*). Labeled neurons and axons were also present in the grey matter. The overall appearance was similar in a homozygous Thy1-YFP-H specimen (not shown). In contrast, in CST-YFP mice the bundle of YFP-labeled axons in the dorsal column was only faintly visible, and was less intense than the background fluorescence in the grey matter (Fig. 6*E*). Individual labeled axons were also not readily discernable in thin horizontal projection (Fig. 6*F*). Thus by the approach that we used, in contrast to labeling with mini-ruby BDA and the axonal labeling in Thy1-YFP-H mice, labeling intensity in CST-YFP mice is not sufficient for axon imaging in cleared tissue.

DISCUSSION

In their original study, Bareyre et al. (2005) suggested that CST-YFP mice would be useful for evaluating regeneration of CST axons because most or all CST axons are labeled without requiring tracer injections. However, regenerative growth distal to a spinal cord injury can involve small numbers of axons extending along routes not normally taken by CST axons (Steward et al., 2003). For definitive identification, it is important that labeling be specific to the CST. Here we show that some YFP-labeled axons extending longitudinally along the spinal cord are not CST axons. YFP-labeled axons were seen outside of regions containing CST axons anterogradely labeled by BDA and most YFP-labeled axons outside the main CST fail to degenerate following a large cortical lesion. Also, following FG injections into the cervical spinal cord, some YFP-positive neurons were retrogradely labeled in the red nucleus and reticular formation. These could account for YFP-labeled non-CST axons in the lateral column. We further demonstrate that axon visualization and tracing, such as could be used to confirm axons are of the CST, are impeded by dense YFP-labeling in CST-YFP mice. Finally, in evaluation of CST-YFP mice for 3D imaging, we found that in comparison to Thy1-YFP-H mice and mice with mini-ruby BDA labeling, the YFP signal from CST-YFP mice is not sufficient for axon imaging in cleared un-sectioned tissue. Overall, these caveats limit the utility of CST-YFP mice for assessing regeneration of CST axons.

YFP labeling of axons and anterograde CST labeling

The pattern of BDA labeling we show in CST-YFP mice is comparable to what has been described previously in mice. The main components of labeled axons are the dCST in the dorsal column, and the dlCST in the dorsal part of the lateral column (Inman and Steward, 2003; Steward et al., 2004). As in our previous studies involving mice, there were few if any BDA-labeled axons in the ventral column in the position of the ventral CST that has been characterized in rats (Brösamle and Schwab, 1997). Thus, CST axons do not follow an unusual course in CST-YFP mice.

YFP-labeled axons were present in the same regions as BDA-labeled CST axons but were also sparsely distributed through the dorsal to ventral lateral column that contains rubrospinal and reticulospinal axons (Jones and Yang, 1985; Inman and Steward, 2003; Ballermann and Fouad, 2006; Liang et al., 2012; Watson and Harrison, 2012). Some of these axons in the DL also appeared thicker than other YFP-labeled axons in the region of BDA-labeled dlCST axons; this is noteworthy because rubrospinal axons are thicker (Powers et al., 2012) than CST axons (Sima and Sourander, 1978). Thus, one possibility is that the YFP-labeled axons outside the normal territory of CST axons are of brainstem origin.

Limited degeneration of YFP-labeled axons outside the dorsal column

The conclusion that some YFP-labeled axons are not part of the CST is also supported by the results following cortical ablation. Large unilateral cortical lesions led to Wallerian degeneration of YFP-labeled axons in the expected locations for the CST (the DC and DL contralateral to the lesion and the ipsilateral VC). In contrast, YFP-labeled axons outside the normal territory of CST axons did not exhibit signs of Wallerian degeneration.

It is noteworthy that there were surprisingly few degenerating YFP-labeled axons in the region of the dlCST contralateral to the lesion. In this regard, there are points to consider. First, the rostro-caudal location selected for analysis and quantification of axons was the mid-cervical spinal cord (approx. C3-C4), and dlCST axons caudally course in fascicles in the dorsolateral grey matter before joining the white matter in the first few cervical levels (Steward et al., 2004). Our counts only included axons in the white matter so dlCST axons in fascicles in the gray matter would not have been counted. Second, dlCST axons might degenerate more slowly than dCST axons. This seems unlikely, however, because signs of beading and fragmentation generally appear by 3–4 days (Lubińska, 1977; Griffin et al., 1992, 1996). Our results are consistent with results of Galley and Clowry (2010) who found that only a few of large YFP-labeled axons in the DL were lost after a neonatal cortical lesion. However, our results and those from Galley and Clowry differ from those of Bareyre et al. (2005), who report that 10% or fewer of YFP-labeled axons in the DL and VC remain after bilateral pyramidotomy in adult CST-YFP mice.

YFP-labeling of rubrospinal neurons, reticulospinal neurons, and neurons in spinal grey matter

Following Fluoro-Gold (FG) injections into the spinal cord, some retrogradely-labeled YFP-positive neurons were present in the red nucleus and reticular formation. Similarly, Galley and Clowry (2010) also found YFP-labeled neurons in the red nucleus and other non-

forebrain regions in juvenile CST-YFP mice, though projections to the spinal cord were not confirmed. In contrast, Bareyre et al. (2005) reported that no YFP-labeled cells were present in the red nucleus, reticular formation, vestibular nucleus, or superior colliculus in adult CST-YFP mice. There is no obvious explanation for this discrepancy, though it is generally recognized that genetic modifiers can change transgenic expression over generations (Allen et al., 1990).

The number of FG and YFP co-labeled neurons varied between mice, ranging from approximately 45–140 rubrospinal neurons and ~20–140 reticulospinal neurons in 1.5 cm of midbrain. Most rubrospinal axons originate from the magnocellular part of the red nucleus, which in mice may have ~2,200 neurons (Liang et al., 2012). In mice, one red nucleus has ~3,200 neurons, and ~2,100 of these have been labeled following injections of FG at C2 (Liang et al., 2012). If there are bilaterally ~4,200 rubrospinal neurons, about 1–3% are YFP-positive in CST-YFP mice. This could account for the YFP-labeled axons in the region of the rubrospinal tract in CST-YFP mice that don't degenerate after cortical lesions. Further, as there may be ~272 non-CST axons labeled with YFP based on our specimens with cortical lesions, YFP-labeled brainstem neurons could account for the majority of non-CST axons labeled with YFP.

YFP-labeled neurons in the spinal cord also extend axons into white matter, accounting for another source of non-CST axons in CST-YFP mice. Tracing axons from these neurons often required superimposing images from adjacent sections. Bareyre et al. (2005) also reported YFP-labeled somata in the grey matter but did not report axons extending into the white matter.

Our finding of YFP labeling of non-CST axons in CST-YFP mice raises caveats for some previous studies involving these mice. For example, enhanced density of YFP-labeled axons post-injury or stroke could be due in part to YFP-labeled non-CST axons (Liu et al., 2009, 2011, 2013). The limitations we show here would have not affected the conclusions of other studies, where analyses of YFP-labeled axons were supplemented with results by additional staining for CST axons (Soulika et al., 2009), only axons in the dorsal column were analyzed (Soulika et al., 2009; Tomassy et al., 2010), analysis was restricted to the brain (Bloom et al., 2007; English et al., 2012), or the observation made was that a type of mouse CST synapse was rare if present (Betley et al., 2009).

Complete tract labeling: too many axons?

As regeneration of the CST may involve few if any axons extending beyond a lesion, complete labeling of the CST optimizes chances to detect rare regenerated axons. YFP-labeling of non-CST axons could mitigate this advantage, but origin from the CST can be confirmed if individual axons can be traced back to the main CST bundle. In CST-YFP mice, however, tracing individual YFP-labeled axons through the dense YFP-labeled arbors is impeded relative to tracing by BDA. This is also noteworthy for regeneration studies as tracing axons back can indicate that potentially regenerated axons branched from injured axons (Tuszynski and Steward, 2012).

Faint labeling limits deep imaging of axons in cleared tissue

Two-photon imaging of rapidly-cleared blocks of spinal cord from CST-YFP mice revealed that individual axons were difficult to resolve relative to those in Thy1-YFP-H mice and mice with mini-ruby BDA labeling. This is probably due to the level of YFP expression in the CST-YFP mice in comparison to Thy1-YFP-H mice. Even immunostaining for YFP produces signal more faint than nascent mini-ruby BDA (Fig. 5). As other studies using mice bred from the Thy1-STOP-YFP line have also used YFP immunostaining (Cheng et al., 2011; Benito-Gonzalez and Alvarez, 2012; Lee et al., 2013; and others), it seems that the issue of faint axon labeling in CST-YFP mice derives from the Thy1-STOP-YFP line. The clearing approach we used permitted rapid clearing (a few hours) appropriate for screening through the unsectioned spinal cord, but immunohistological methods with clearing such as CLARITY may solve the problem of inadequate axon visualization, though with a much longer processing timecourse (Spence et al., 2014; Tomer et al., 2014; Yang et al., 2014).

Caveats of Emx1 and breeding in the Cre-Lox system for specific labeling

CST-YFP mice are generated in a Cre-Lox breeding system as the progeny of one parent mouse with Emx1-driven Cre recombinase (Emx-Cre) and one parent mouse with a floxed STOP cassette following a neuronal Thy1 promoter and preceding *YFP* (Thy1-STOP-YFP). In offspring CST-YFP mice, YFP expression is achieved by Cre-mediated excision of the STOP cassette driven by Emx1 in Thy1-STOP-YFP neurons (Briata et al., 1996; Buffelli et al., 2003; Bareyre et al., 2005). As Emx1 is a forebrain transcription factor in development (Simeone et al., 1992; Briata et al., 1996), this mouse is designed to yield permanent labeling of forebrain neurons, including the cells of origin of the CST.

In a Cre-Lox breeding system, however, transient Cre expression can result in permanent genetic excision. This may explain labeling of non-CST axons in CST-YFP mice. Additionally, Emx1 is not specific to the embryonic forebrain; Emx1 has also been identified in the developing embryonic mesencephalon (Briata et al., 1996), and Emx1-based Cre expression results in scattered labeling of adult midbrain cells in a LacZ reporter mouse (Mouse Genome Informatics website of The Jackson Laboratory, http://www.informatics.jax.org, accessed Nov. 2014, RRID: nif-0000–00096). The non-forebrain expression of Emx1 could account for YFP-labeled cells in the red nucleus and midbrain reticular formation in CST-YFP mice.

In future generation of genetically-labeled mice for experiments requiring stringent tract or tissue specificity such as is needed for studying CST regeneration, we anticipate that it will be necessary to avoid genetic drivers that result in permanent nonspecific labeling.

Supplementary Material

Refer to Web version on PubMed Central for supplementary material.

ACKNOWLEDGMENTS

We thank Joe Dynes, Rachel Thong, David Sengmany, and Maria Ramos-Masa for assistance with imaging and technical assistance, Karla McHale and Kelli Sharp for surgical assistance, Kelly Yee for immunohistochemical guidance, Joe Bonner and Gail Lewandowski for feedback and advice, and Abraham Chiu, Zachary Gallaher, Maya

Hatch, and Kelly Yee for performing the axon tracing task. We are grateful to Emiliana Borrelli, and the W.M. Keck Nano-Imaging Laboratory (W.M.KNIL) and Laboratory for Fluorescence Dynamics (LFD) for use of their confocal microscopes.

This work was supported by National Institutes of Health grant NS047718 (O.S.), National Institutes of Health fellowship F31NS070558 (R.W.), the Roman Reed Spinal Cord Injury Research Fund of California, and private donations to the Reeve-Irvine Research Center. The W.M. KNIL and LFD are supported by the W.M. Keck Foundation, National Center for Research Resources grant 5P41RR003155-27, National Institute of General Medical Sciences grant 8P41GM103540, and the University of California at Irvine.

REFERENCES

Abercrombie M. Estimation of nuclear population from microtome sections. Anat Rec. 1946; 94:239–247. [PubMed: 21015608]

Allen ND, Norris ML, Surani MA. Epigenetic control of transgene expression and imprinting by genotype-specific modifiers. Cell. 1990; 61:853–861. [PubMed: 2111735]

Ambalavanar R, Morris R. Fluoro-Gold injected either subcutaneously or intravascularly results in extensive retrograde labelling of CNS neurones having axons terminating outside the blood-brain barrier. Brain Res. 1989; 505:171–175. [PubMed: 2611674]

Ballermann M, Fouad K. Spontaneous locomotor recovery in spinal cord injured rats is accompanied by anatomical plasticity of reticulospinal fibers. Eur J Neurosci. 2006; 23:1988–1996. [PubMed: 16630047]

Bareyre FM, Kerschensteiner M, Misgeld T, Sanes JR. Transgenic labeling of the corticospinal tract for monitoring axonal responses to spinal cord injury. Nat Med. 2005; 11:1355–1360. [PubMed: 16286922]

Beirowski B, Nógrádi A, Babetto E, Garcia-Alias G, Coleman MP. Mechanisms of axonal spheroid formation in central nervous system Wallerian degeneration. J Neuropathol Exp Neurol. 2010; 69:455–472. [PubMed: 20418780]

Benito-Gonzalez A, Alvarez FJ. Renshaw cells and Ia inhibitory interneurons are generated at different times from p1 progenitors and differentiate shortly after exiting the cell cycle. J Neurosci. 2012; 32:1156–1170. [PubMed: 22279202]

Betley JN, Wright CVE, Kawaguchi Y, Erdélyi F, Szabó G, Jessell TM, Kaltschmidt JA. Stringent specificity in the construction of a GABAergic presynaptic inhibitory circuit. Cell. 2009; 139:161–174. [PubMed: 19804761]

Bloom AJ, Miller BR, Sanes JR, DiAntonio A. The requirement for Phr1 in CNS axon tract formation reveals the corticostriatal boundary as a choice point for cortical axons. Genes Dev. 2007; 21:2593–2606. [PubMed: 17901218]

Briata P, Di Blas E, Gulisano M, Mallamaci A, Iannone R, Boncinelli E, Corte G. EMX1 homeoprotein is expressed in cell nuclei of the developing cerebral cortex and in the axons of the olfactory sensory neurons. Mech Dev. 1996; 57:169–180. [PubMed: 8843394]

Brösamle C, Schwab ME. Cells of origin, course, and termination patterns of the ventral, uncrossed component of the mature rat corticospinal tract. J Comp Neurol. 1997; 386:293–303. [PubMed: 9295153]

Buffelli M, Burgess RW, Feng G, Lobe CG, Lichtman JW, Sanes JR. Genetic evidence that relative synaptic efficacy biases the outcome of synaptic competition. Nature. 2003; 424:430–434. [PubMed: 12879071]

Cheng X, Li Y, Huang Y, Feng X, Feng G, Xiong Z-Q. Pulse labeling and long-term tracing of newborn neurons in the adult subgranular zone. Cell Res. 2011; 21:338–349. [PubMed: 20938464]

Chung K, Wallace J, Kim S-Y, Kalyanasundaram S, Andalman AS, Davidson TJ, Mirzabekov JJ, Zalocusky KA, Mattis J, Denisin AK, Pak S, Bernstein H, Ramakrishnan C, Grosenick L, Gradinaru V, Deisseroth K. Structural and molecular interrogation of intact biological systems. Nature. 2013; 497:332–337. [PubMed: 23575631]

Coonan JR, Greferath U, Messenger J, Hartley L, Murphy M, Boyd AW, Dottori M, Galea MP, Bartlett PF. Development and reorganization of corticospinal projections in EphA4 deficient mice. J Comp Neurol. 2001; 436:248–262. [PubMed: 11438928]

Dado RJ, Burstein R, Cliffer KD, Giesler GJ. Evidence that Fluoro-Gold can be transported avidly through fibers of passage. Brain Res. 1990; 533:329–333. [PubMed: 1705157]

English CN, Vigers AJ, Jones KR. Genetic evidence that brain-derived neurotrophic factor mediates competitive interactions between individual cortical neurons. Proc Natl Acad Sci USA. 2012; 109:19456–19461. [PubMed: 23129644]

Ertürk A, Becker K, Jährling N, Mauch CP, Hojer CD, Egen JG, Hellal F, Bradke F, Sheng M, Dodt H-U. Three-dimensional imaging of solvent-cleared organs using 3DISCO. Nat Protoc. 2012a; 7:1983–1995. [PubMed: 23060243]

Ertürk A, Mauch CP, Hellal F, Förstner F, Keck T, Becker K, Jährling N, Steffens H, Richter M, Hübener M, Kramer E, Kirchhoff F, Dodt HU, Bradke F. Three-dimensional imaging of the unsectioned adult spinal cord to assess axon regeneration and glial responses after injury. Nat Med. 2012b; 18:166–171. [PubMed: 22198277]

Galley S, Clowry GJ. Plasticity to neonatal sensorimotor cortex injury. Transl Neurosci. 2010; 1:16–23.

Gorski JA, Talley T, Qiu M, Puelles L, Rubenstein JL, Jones KR. Cortical excitatory neurons and glia, but not GABAergic neurons, are produced in the Emx1-expressing lineage. JNeurosci. 2002; 22:6309–6314. [PubMed: 12151506]

Griffin JW, George EB, Chaudhry V. Wallerian degeneration in peripheral nerve disease. Baillieres Clin Neurol. 1996; 5:65–75. [PubMed: 8732200]

Griffin JW, George R, Lobato C, Tyor WR, Yan LC, Glass JD. Macrophage responses and myelin clearance during Wallerian degeneration: relevance to immune-mediated demyelination. J Neuroimmunol. 1992; 40:153–165. [PubMed: 1430148]

Guillery R. On counting and counting errors. J Comp Neurol. 2002; 447:1–7. [PubMed: 11967890]

Hama H, Kurokawa H, Kawano H, Ando R, Shimogori T, Noda H, Fukami K, Sakaue-Sawano A, Miyawaki A. Scale: a chemical approach for fluorescence imaging and reconstruction of transparent mouse brain. Nat Neurosci. 2011; 14:1481–1488. [PubMed: 21878933]

Inman DM, Steward O. Ascending sensory, but not other long-tract axons, regenerate into the connective tissue matrix that forms at the site of a spinal cord injury in mice. J Comp Neurol. 2003; 462:431–449. [PubMed: 12811811]

Jones BE, Yang TZ. The efferent projections from the reticular formation and the locus coeruleus studied by anterograde and retrograde axonal transport in the rat. J Comp Neurol. 1985; 242:56–92. [PubMed: 2416786]

Kalil K, Schneider GE. Retrograde cortical and axonal changes following lesions of the pyramidal tract. Brain Res. 1975; 89:15–27. [PubMed: 1148840]

Ke M-T, Fujimoto S, Imai T. SeeDB: a simple and morphology-preserving optical clearing agent for neuronal circuit reconstruction. Nat Neurosci. 2013; 16:1154–1161. [PubMed: 23792946]

Kerschensteiner M, Schwab ME, Lichtman JW, Misgeld T. In vivo imaging of axonal degeneration and regeneration in the injured spinal cord. Nat Med. 2005; 11:572–577. [PubMed: 15821747]

Kuwajima T, Sitko AA, Bhansali P, Jurgens C, Guido W, Mason C. ClearT: a detergent- and solvent-free clearing method for neuronal and non-neuronal tissue. Development. 2013; 140:1364–1368. [PubMed: 23444362]

Lang C, Guo X, Kerschensteiner M, Bareyre FM. Single collateral reconstructions reveal distinct phases of corticospinal remodeling after spinal cord injury. PLoS One. 2012; 7:e30461. [PubMed: 22291960]

Lee N, Rydyznski CE, Spearry RP, Robitz R, Maclennan AJ. The contribution of ciliary neurotrophic factor receptors to adult motor neuron survival in vivo is specific to insult type and distinct from that for embryonic motor neurons. J Comp Neurol. 2013; 521:3217–3225. [PubMed: 23695797]

Liang H, Paxinos G, Watson C. Projections from the brain to the spinal cord in the mouse. Brain Struct Funct. 2011; 215:159–186. [PubMed: 20936329]

Liang H, Paxinos G, Watson C. The red nucleus and the rubrospinal projection in the mouse. Brain Struct Funct. 2012; 217:221–232. [PubMed: 21927901]

Liu K, Lu Y, Lee JK, Samara R, Willenberg R, Sears-Kraxberger I, Tedeschi A, Park KK, Jin D, Cai B, Xu B, Connolly L, Steward O, Zheng B, He Z. PTEN deletion enhances the regenerative ability of adult corticospinal neurons. Nat Neurosci. 2010; 13:1075–1081. [PubMed: 20694004]

Liu Z, Chopp M, Ding X, Cui Y, Li Y. Axonal remodeling of the corticospinal tract in the spinal cord contributes to voluntary motor recovery after stroke in adult mice. Stroke. 2013; 44:1951–1956. [PubMed: 23696550]

Liu Z, Li Y, Zhang RL, Cui Y, Chopp M. Bone marrow stromal cells promote skilled motor recovery and enhance contralesional axonal connections after ischemic stroke in adult mice. Stroke. 2011; 42:740–744. [PubMed: 21307396]

Liu Z, Zhang RL, Li Y, Cui Y, Chopp M. Remodeling of the corticospinal innervation and spontaneous behavioral recovery after ischemic stroke in adult mice. Stroke. 2009; 40:2546–2551. [PubMed: 19478220]

Lubińska L. Early course of Wallerian degeneration in myelinated fibres of the rat phrenic nerve. Brain Res. 1977; 130:47–63. [PubMed: 884520]

Mantyh PW, Peschanski M. Spinal projections from the periaqueductal grey and dorsal raphe in the rat, cat and monkey. Neuroscience. 1982; 7:2769–2776. [PubMed: 7155351]

Naumann T, Härtig W, Frotscher M. Retrograde tracing with Fluoro-Gold: different methods of tracer detection at the ultrastructural level and neurodegenerative changes of back-filled neurons in long-term studies. J Neurosci Methods. 2000; 103:11–21. [PubMed: 11074092]

Nielson JL, Strong MK, Steward O. A reassessment of whether cortical motor neurons die following spinal cord injury. J Comp Neurol. 2011; 519:2852–2869. [PubMed: 21618218]

Paxinos, G. Compact. 2nd ed.. Amsterdam; Boston: Elsevier Academic Press; 2004. The mouse brain in stereotaxic coordinates.

Powers BE, Lasiene J, Plemel JR, Shupe L, Perlmutter SI, Tetzlaff W, Horner PJ. Axonal thinning and extensive remyelination without chronic demyelination in spinal injured rats. J Neurosci. 2012; 32:5120–5125. [PubMed: 22496557]

Preibisch S, Saalfeld S, Tomancak P. Globally optimal stitching of tiled 3D microscopic image acquisitions. Bioinformatics. 2009; 25:1463–1465. [PubMed: 19346324]

Qu S, Ondo W, Zhang X, Xie W, Pan T, Le W. Projections of diencephalic dopamine neurons into the spinal cord in mice. Experimental Brain Research. 2006; 168:152–156. [PubMed: 16044299]

Rasband, W. ImageJ. U. S. National Institutes of Health, Bethesda, Maryland, USA. 1997. Available from: http://rsb.info.nih.gov/ij/

Schaefer AM, Sanes JR, Lichtman JW. A compensatory subpopulation of motor neurons in a mouse model of amyotrophic lateral sclerosis. J Comp Neurol. 2005; 490:209–219. [PubMed: 16082680]

Schmued LC, Beltramino C, Slikker W Jr. Intracranial injection of Fluoro-Gold results in the degeneration of local but not retrogradely labeled neurons. Brain Res. 1993; 626:71–77. [PubMed: 8281454]

Schmued LC, Fallon JH. Fluoro-Gold: a new fluorescent retrograde axonal tracer with numerous unique properties. Brain Res. 1986; 377:147–154. [PubMed: 2425899]

Sima A, Sourander P. The effect of pre-and postnatal undernutrition on axonal growth and myelination of central motor fibers. Acta Neuropathol. 1978; 42:15–18. [PubMed: 654874]

Simeone A, Gulisano M, Acampora D, Stornaiuolo A, Rambaldi M, Boncinelli E. Two vertebrate homeobox genes related to the Drosophila empty spiracles gene are expressed in the embryonic cerebral cortex. EMBO J. 1992; 11:2541–2550. [PubMed: 1352754]

Soulika AM, Lee E, McCauley E, Miers L, Bannerman P, Pleasure D. Initiation and progression of axonopathy in experimental autoimmune encephalomyelitis. J Neurosci. 2009; 29:14965–14979. [PubMed: 19940192]

Spence RD, Kurth F, Itoh N, Mongerson CRL, Wailes SH, Peng MS, MacKenzie-Graham AJ. Bringing CLARITY to gray matter atrophy. Neuroimage. 2014; 101:625–632. [PubMed: 25038439]

Steward O, Zheng B, Ho C, Anderson K, Tessier-Lavigne M. The dorsolateral corticospinal tract in mice: an alternative route for corticospinal input to caudal segments following dorsal column lesions. J Comp Neurol. 2004; 472:463–477. [PubMed: 15065120]

Steward O, Zheng B, Tessier-Lavigne M. False resurrections: distinguishing regenerated from spared axons in the injured central nervous system. J Comp Neurol. 2003; 459:1–8. [PubMed: 12629662]

Steward O, Zheng B, Tessier-Lavigne M, Hofstadter M, Sharp K, Yee KM. Regenerative growth of corticospinal tract axons via the ventral column after spinal cord injury in mice. J Neurosci. 2008; 28:6836–6847. [PubMed: 18596159]

Tomassy GS, De Leonibus E, Jabaudon D, Lodato S, Alfano C, Mele A, Macklis JD, Studer M. Area-specific temporal control of corticospinal motor neuron differentiation by COUP-TFI. Proc Natl Acad Sci USA. 2010; 107:3576–3581. [PubMed: 20133588]

Tomer R, Ye L, Hsueh B, Deisseroth K. Advanced CLARITY for rapid and high-resolution imaging of intact tissues. Nat Protoc. 2014; 9:1682–1697. [PubMed: 24945384]

Tuszynski MH, Steward O. Concepts and methods for the study of axonal regeneration in the CNS. Neuron. 2012; 74:777–791. [PubMed: 22681683]

Waller A. Experiments on the section of the glossopharyngeal and hypoglossal nerves of the frog, and observations of the alterations produced thereby in the structure of their primitive fibres. Philos Trans R Soc London. 1850; 140:423–429.

Watson C, Harrison M. The location of the major ascending and descending spinal cord tracts in all spinal cord segments in the mouse: actual and extrapolated. Anat Rec. 2012; 295:1692–1697.

Yang B, Treweek JB, Kulkarni RP, Deverman BE, Chen C-K, Lubeck E, Shah S, Cai L, Gradinaru V. Single-cell phenotyping within transparent intact tissue through whole-body clearing. Cell. 2014; 158:945–958. [PubMed: 25088144]

Zheng B, Lee JK, Xie F. Genetic mouse models for studying inhibitors of spinal axon regeneration. Trends Neurosci. 2006; 29:640–646. [PubMed: 17030430]

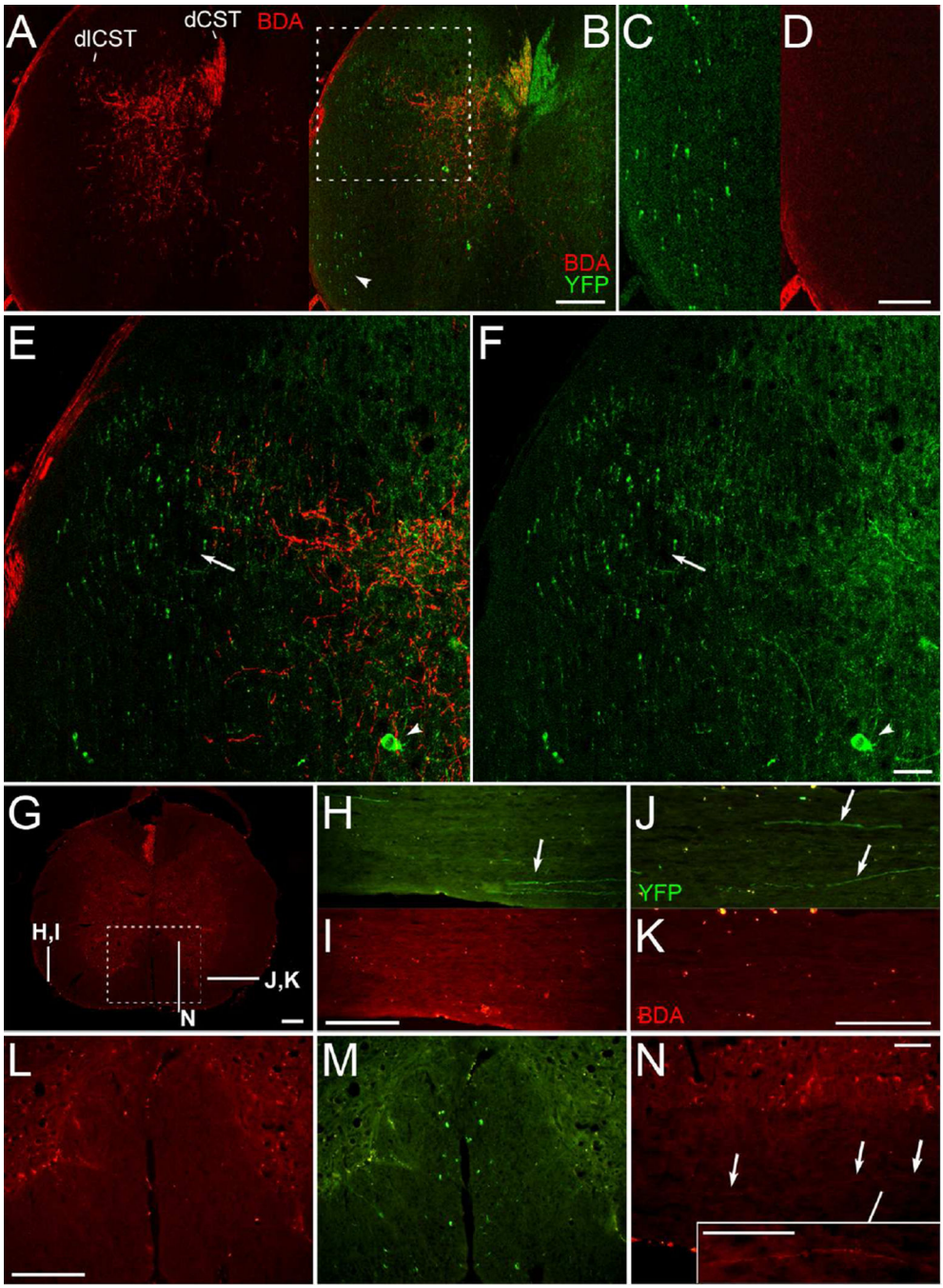

Figure 1.

YFP-labeled axons are in areas of the spinal cord that do not contain anterogradely-labeled CST axons. ***A-F***, Confocal images of a spinal cord cross section with amplified BDA signal. BDA labeled CST axons (***A***) are illustrated relative to YFP labeling (***B***) following BDA injections into the right sensorimotor cortex. The ventral lateral white matter (arrowhead, ***B***) is enlarged in ***C*** and ***D***; note the absence of BDA-labeled axons in ***D***. The dorsolateral column (boxed region in ***B***) is shown in higher magnification in ***E-F***; arrowheads indicate YFP-labeled neurons in the grey matter; arrows indicate the region of the rubrospinal tract,

which overlaps with the dlCST. Note that some YFP-labeled axons in this region are distinctly thicker in appearance. ***G***, Cross section with mini-ruby BDA labeling and indicated locations of sections shown in ***H-N***. ***H-K***, Sections in ventral lateral white matter with YFP-labeled axons (arrows in ***H-J***) and as shown for BDA labeling (***I,K***); note the bilateral absence of BDA-labeled axons. ***L-M***, BDA (***L***) and YFP labeling (***M***) in the ventral column (boxed region from ***G***). ***N***, A BDA-labeled axon coursing longitudinally in the ventral column ipsilateral to the injected cortex, as seen in one of 14 mice. The inset in ***N*** has been further enhanced for contrast. This figure with magenta-green confocal panels is available as Supplementary Figure S1. dCST, dorsal corticospinal tract; dlCST, dorsolateral CST. Scale bars, 200 μm (***A-B, G-M***), 100 μm (***C-D, N*** and inset), 50 μm (***E-F***).

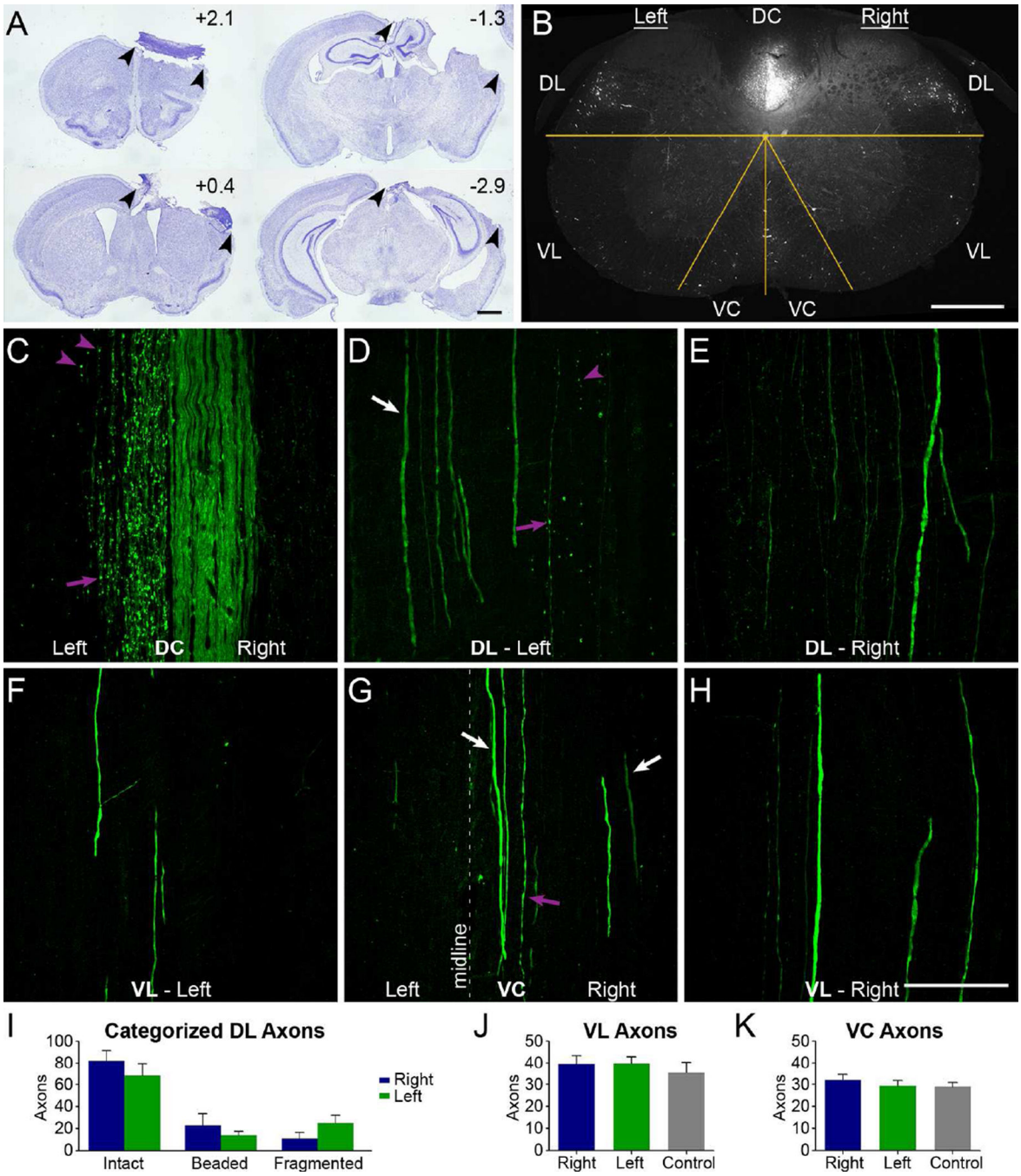

Figure 2.

Ablation of the sensorimotor cortex does not lead to degeneration of YFP axons outside the main CST. ***A***, Sections from a representative specimen with a large lesion to ablate CST origins from the right cortex; arrowheads show lesion extent. Rostro-caudal distances of each section from bregma are indicated. ***B***, Confocal cross section of cervical spinal cord 1 week after unilateral cortical ablation. The overlaid yellow lines distinguish the different white matter regions where axons were quantified. ***C-H***, Longitudinal sections of dorsal (***C-E***) and ventral (***F-H***) cervical spinal cord, by regions as indicated in ***B***. Purple arrows

indicate beaded axons; arrowheads indicate fragmented axons; white arrows indicate intact axons. Note the intact axons in the left DL (***D***) and right VC (***G***), as well as bilaterally in the VL (***F, H***). ***I***, Quantification of categorized axons in the DL in longitudinal sections in mice with a cortical lesion. Differences between sides for the intact, beaded, and fragmented axons were not statistically significant (all $p > 0.05$, Bonferroni post-hoc tests following 2-way mixed-model ANOVA). ***J, K***, Quantification in cross sections of the overall number of right or left axons in mice with a cortical lesion or axons of control mice in the VL (***J***) and VC (***K***), with no respective significant differences (both $p>0.6$, ANOVAs). The image in ***C*** is a single-plane confocal capture and ***D-H*** are confocal projections. DC, dorsal column; DL, dorsolateral white matter; VC, ventral column; VL, ventral lateral column. Data are mean + SEM. Scale bars, 1 mm (***A***), 400 μm (***B***), 100μm (***C-H***).

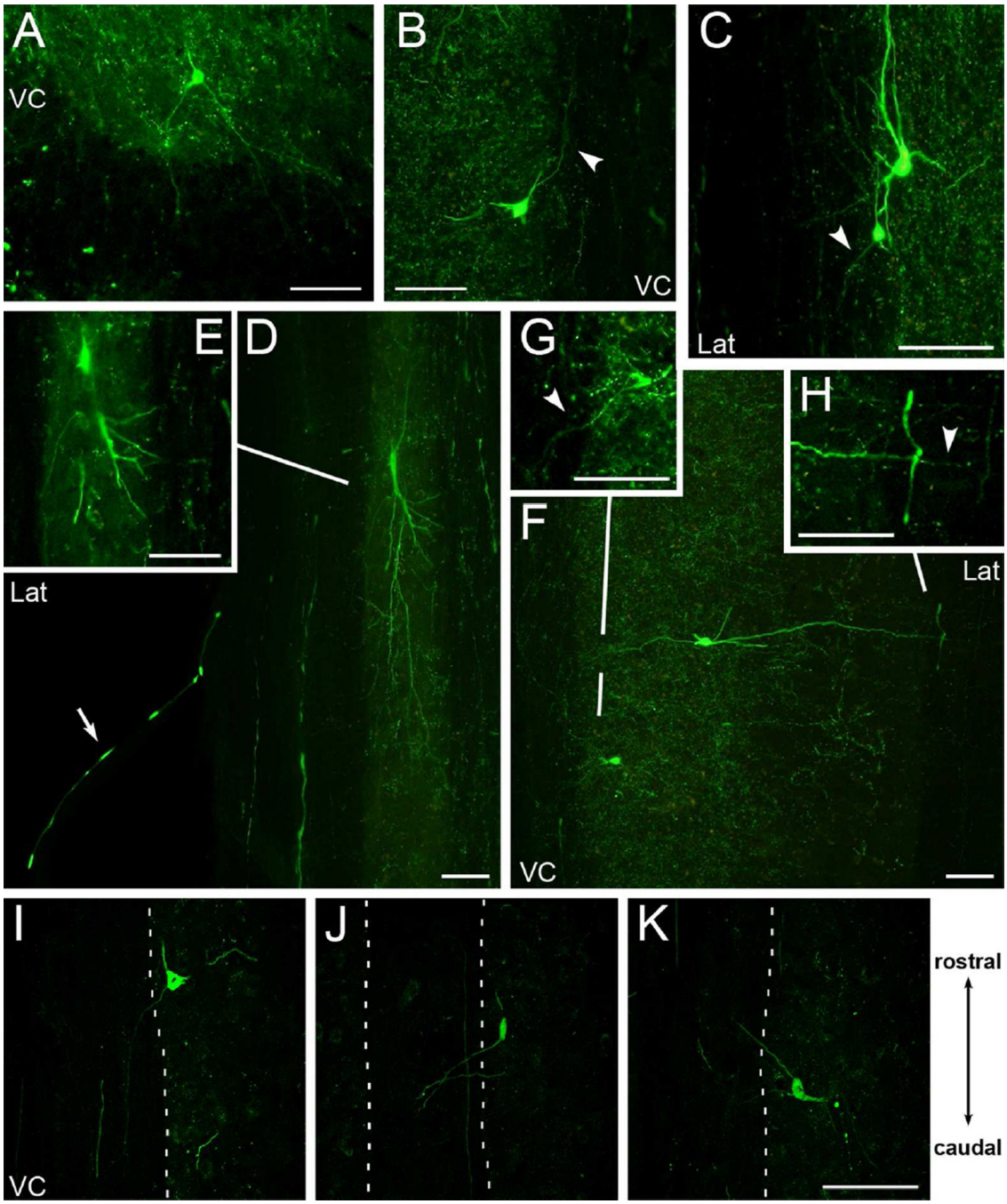

Figure 3.

Some YFP-labeled cells in the spinal cord project into the white matter. ***A***, Cross section of cervical spinal cord showing a YFP-labeled cell in the ventral grey matter with projections extending into the ventral white matter. ***B-H***, Examples of YFP-labeled cells in horizontal sections extending projections into the ventral medial and lateral white matter of the cervical (***B, F-H***) and thoracic (***C-E***) spinal cord. Arrowheads highlight some YFP-labeled projections. Each image panel is a projected overlay of 2 adjacent tissue sections except for the images of single tissue sections in inset panels ***E*** and ***G***. Inset panels were further

adjusted for brightness and contrast to enhance detail. In ***D***, also note the YFP-labeled axon coursing in the ventral root (arrow) and lateral white matter. ***I-K***, Selected confocal projections from mice with large cortical lesions showing YFP-labeled cells in the spinal cord with projections extending both caudally (***I-J***), and rostrally (***K***) in the white matter of the ventral column. VC, ventral column; Lat, lateral white matter. Rostral-caudal diagram applies to ***B-K***. Scale bars, 100μm.

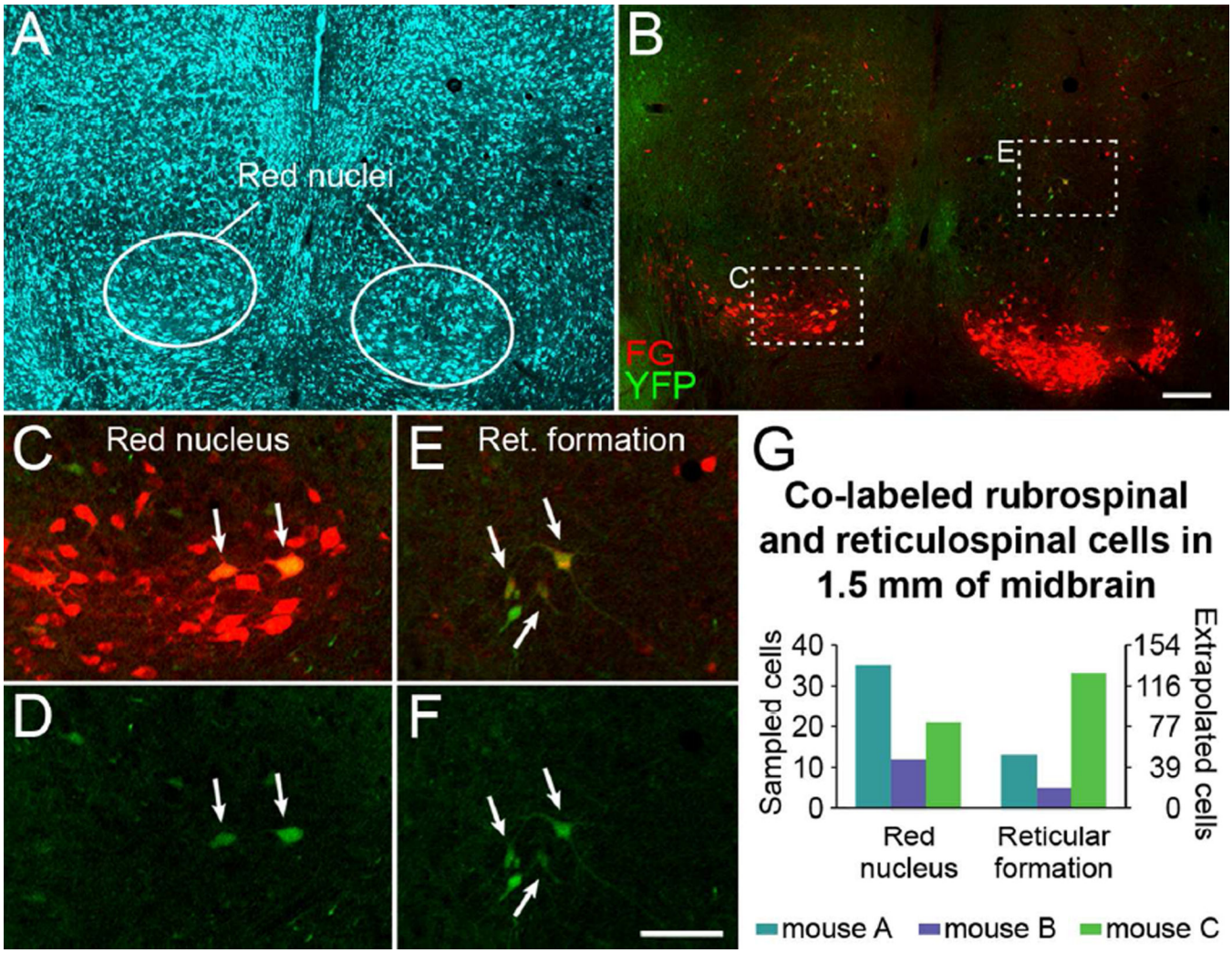

Figure 4.

Some brainstem neurons that project to the spinal cord express YFP. ***A***, Fluorescent Nissl-like labeling (NeuroTrace®) in the midbrain in a mouse that had FG injected into the spinal cord to retrogradely label supraspinal neurons. ***B***, FG and YFP labeling in the midbrain (same section as ***A***). ***C-F***, Merged FG and YFP imaging (***C, E***) and YFP imaging alone (***D, F***) in the red nucleus (***C, D***) and reticular formation (***E, F***). Note the FG-labeled rubrospinal and reticulospinal neurons that are YFP-positive (arrows). ***G***, Quantification of sampled YFP and FG co-labeled rubrospinal and reticulospinal neurons through 1.5 mm of midbrain in 3 mice. ***A-F*** are single plane confocal images. A magenta-green version of this figure is available as Supplementary Figure S2. FG, Fluoro-Gold; Ret. formation, reticular formation. Scale bars, 200 μm (***A-B***), 100 μm (***C-F***).

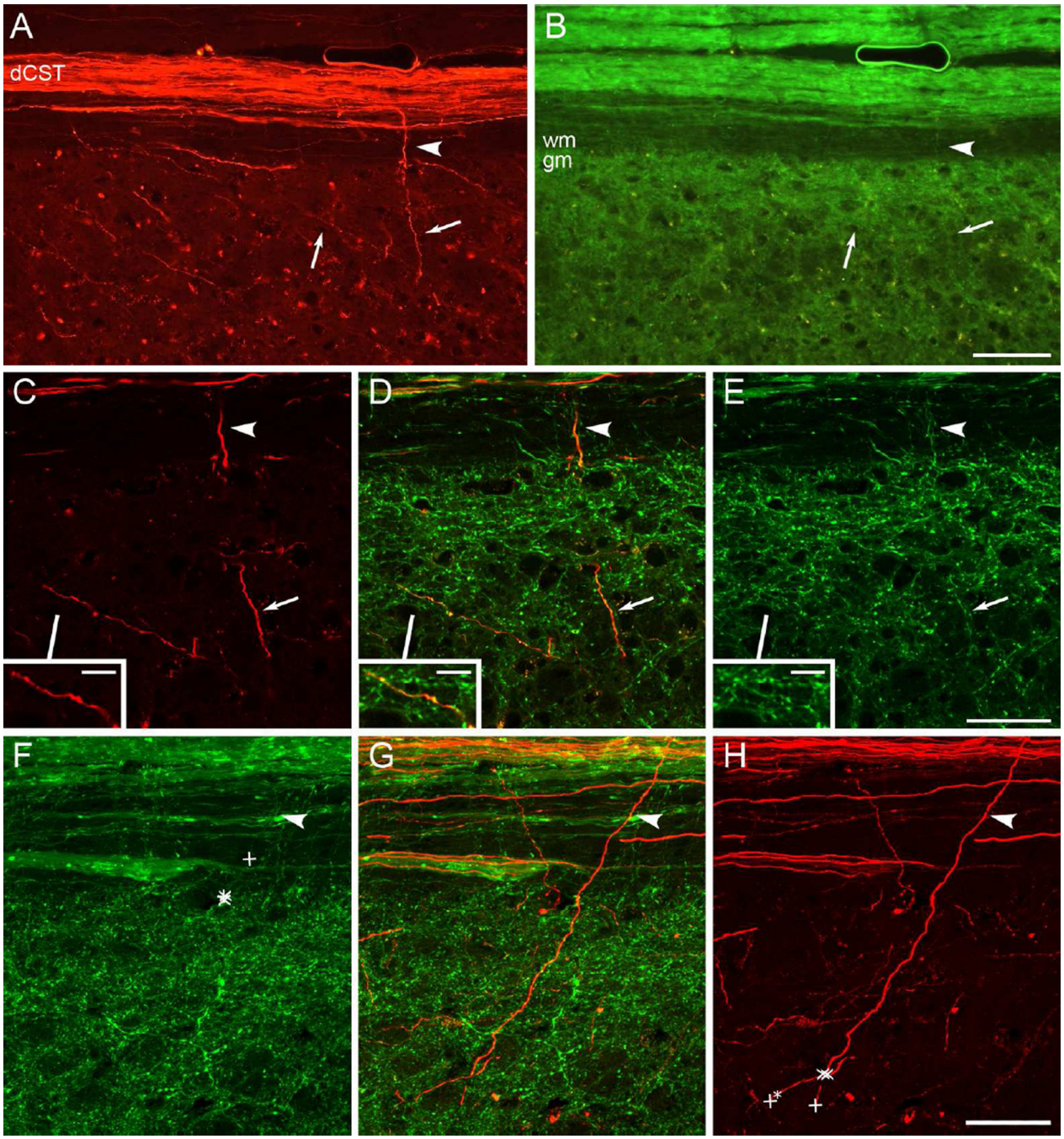

Figure 5.

Dense and faint YFP labeling impedes individual axon visualization and tracing. ***A-B***, Epifluorescent images at 20X magnification showing individual BDA-labeled CST axons in the white matter (arrowhead, ***A***) and grey matter (arrows, ***A***) and YFP labeling in the same section (***B***). Note the faint labeling of individual axons with YFP. ***C-E***, Confocal images at 40X magnification showing CST axons labeled with BDA from ***A*** (***C***, arrowhead, arrow and inset) are co-labeled with YFP (***D, E***). ***F-H***, Confocal projections of one axon originating from the dCST and traced by experienced (X) and novice (+) axon tracers. Individuals were

instructed to trace the axon from the arrowhead to the best of their ability within the stack of 40X confocal images, as visualized first by YFP and then BDA. Note that none of the YFP-based tracings extend beyond the grey matter interface (***F***), whereas all the BDA-based tracings extend into the grey matter (***H***). One novice tracer continued tracing to an incorrect axon segment under visualization with BDA (+* in ***H***). This figure with magenta-green confocal panels is available as Supplementary Figure S3. dCST, dorsal corticospinal tract; gm, grey matter; wm, white matter. Scale bars, 100 μm (***A***-***B***), 50 μm (***C***-***H***), 10 μm (***C***-***E*** insets).

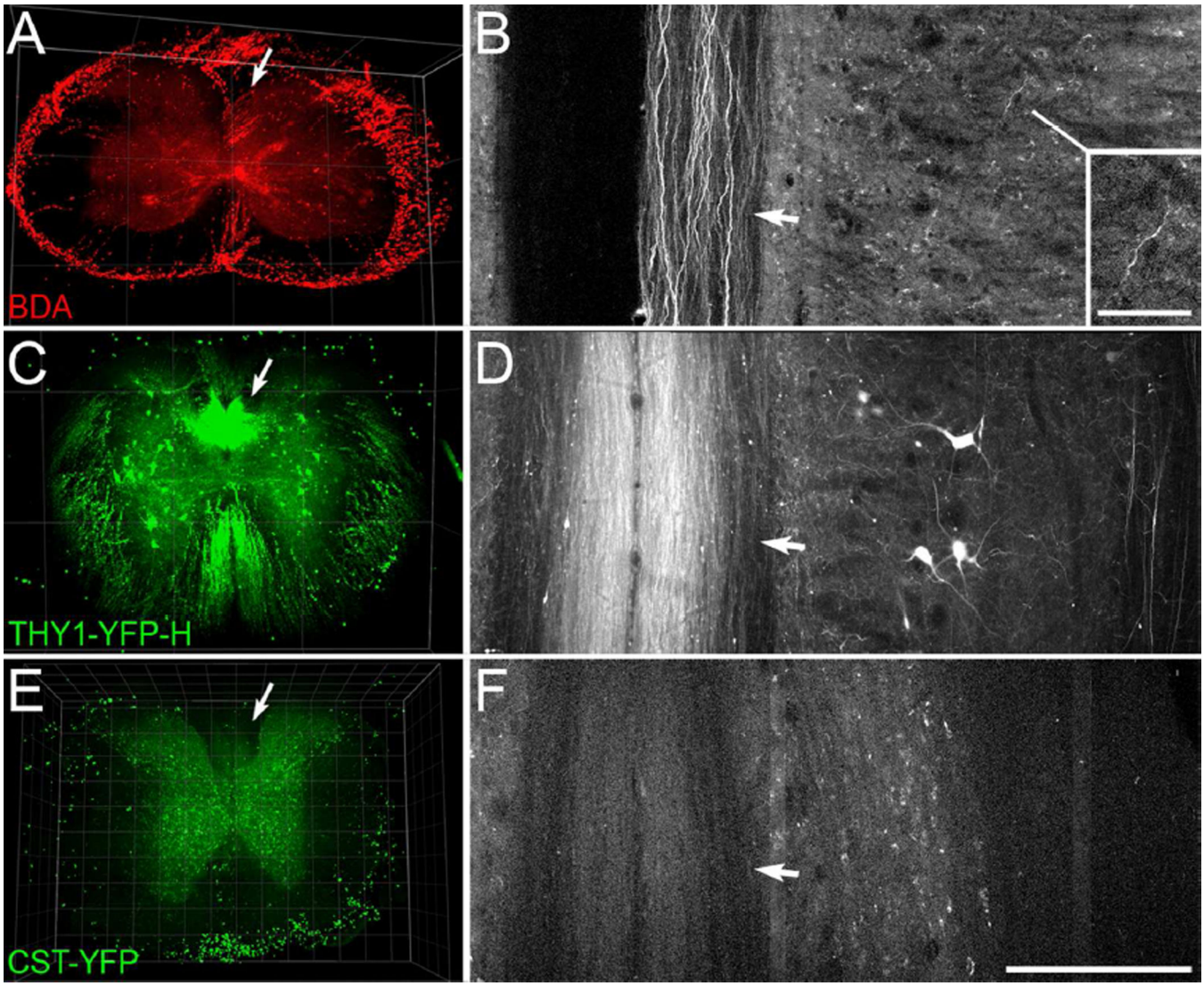

Figure 6.

3D imaging of cleared blocks of spinal cord from a mouse with BDA-labeled CST axons, a Thy1-YFP-H mouse, and a CST-YFP mouse. ***A-B***, A 3D view through 482 μm of cervical spinal cord (***A***) and horizontal projection through 6μm of the dorsal column (***B***) show visible BDA-labeled axons in the dorsal CST (arrows), rostral to a spinal cord injury. This tissue is from a *Pten*$^{fl/fl}$ mouse that had received cortical injections of AAV-Cre and mini-ruby BDA injections into the left cortex. Note the visible individual axons in horizontal projection in the dorsal column (arrow, ***B***), and in the grey matter (inset, ***B***). ***C-D***, A 3D view through 450 μm of spinal cord (***C***) and 6 μm horizontal projection in the dorsal column (***D***) from a hemizygous Thy1-YFP H mouse. Note the strong signal intensity of axons in the dorsal column (arrows) as well as individual axons distributed through the spinal cord. ***E-F***, A 3D view through 400 μm of a block of thoracic spinal cord (***E***) and 6 μm horizontal projection though the dorsal column (***F***) from a CST-YFP mouse. Note that the signal from axons in the dorsal column (arrows) is lower than that of the grey matter background. Scan settings were the same as for the block of spinal cord from the Thy1-YFP-H mouse shown in ***C-D***.

Fluorescence of the outer rim in ***A*** and ventral rim in ***E*** is artifact presumably from remaining sub-dural vasculature. Laser excitation was 850 nm for the specimen with BDA (***A-B***), and 950 nm for the CST-YFP and Thy1-YFP-H mouse (***C-F***). Grid spacing, 500 μm (***A, C***), 100 μm (***E***). Scale bar, 200 μm (***B, D, F***), 50 μm (***B***, inset).

Table 1

Axon Tracing Task Results

Lengths of tracings of designated axons as visualized first by YFP, then by BDA. In three cases individuals' tracing ended on incorrect YFP-labeled axons (*), and this occurred in one case based on BDA-labeling, from a novice axon tracer. Overall tracings based on visualization by YFP were significantly shorter than tracings by visualization by BDA (p = 0.0402, two-tailed paired t-test), as were tracings in which incorrectly traced axons were excluded (p = 0.0494, two-tailed paired t-test).

	YFP tracing			BDA tracing		
	Axon 1	Axon 2	Axon 3	Axon 1	Axon 2	Axon 3
Tracer 1: experienced	15.9*	96.6*	58.0	172.6	122.9	184.5
Tracer 2: novice	12.2	8.5*	32.4	170.5	157.3	214.7*
Tracer 2: novice	26.6	61.4	59.4	171.9	124.3	202.2
Tracer 4: experienced	32.1	78.7	59.6	159.1	123.9	184.5